Solar Physics
DOI: 10.1007/•••••-•••-•••-••••-•

CoMP observations of Coronal Mass Ejections

H. Tian[1] · **S. Tomczyk**[2] · **S. W. McIntosh**[2] · **C. Bethge**[2] · **L. Sitongia**[2] · **G. de Toma**[2] · **P. Judge**[2] · **S. Gibson**[2] ·

Abstract CoMP measures not only the polarization of coronal emission, but also the full radiance profiles of coronal emission lines. For the first time, CoMP observations provide high-cadence image sequences of the coronal line intensity, Doppler shift and line width simultaneously in a large field of view. By studying the Doppler shift and line width we may explore more of the physical processes of CME initiation and propagation. Here we identify a list of CMEs observed by CoMP and present the first results of these observations. Our preliminary analysis shows that CMEs are usually associated with greatly increased Doppler shift and enhanced line width. These new observations provide not only valuable information to constrain CME models and probe various processes during CMEs, but also offer a cheap and low-risk means of space weather forecasting.

Keywords: Active Regions, Coronal Mass Ejections, Flares, Magnetic fields, Waves

1. Introduction

Coronal mass ejections (CMEs) are probably the most important sources of adverse space weather effects (e.g., Gosling *et al.*, 1991, Wang *et al.*, 2002,Zhang *et al.*, 2007). Using mainly white-light coronagraphs, observations of CMEs are now made routinely both on the ground and in space. These instruments measure the polarized or total brightness of the corona and CMEs are usually identified as large-scale disturbances in the coronal intensity image sequences. White-light coronagraphs such as MK4 in the Mauna Loa Solar Observatory (MLSO) and the Large Angle Spectrometric Coronagraph (LASCO) (Brueckner *et al.*, 1995) onboad the Solar and Heliospheric Observatory (SOHO) have made great contribution to our understanding of the initiation and propagation of CMEs.

Spectroscopic observations of coronal emission lines could provide valuable information on the properties and dynamics of CMEs (e.g.,Harrison *et al.*, 2003,McIntosh, de Pontieu, and Leamon, 2010,Tian *et al.*, 2012). However, conventional

[1]Harvard-Smithsonian Center for Astrophysics. email: htian@head.cfa.harvard.edu or hui.tian@cfa.harvard.edu
[2]High Altitude Observatory, National Center for Atmospheric Research. email: tomczyk@ucar.edu

slit spectrographs can only observe a small region of the Sun through raster scan. In addition, repeated observations of the same region can only be done at a low cadence (e.g., about 5 minutes for HINODE/EIS) because it takes minutes or even hours to scan the region. A filter instrument, on the other hand, can provide high-cadence observations of a large field of view in the solar corona, thus offering significant advantages over a spectrograph when observing large-scale solar eruptions like CMEs. The LASCO C1 instrument might be considered as one of such instruments. However, it took minutes to record a complete spectrum (Mierla *et al.*, 2005) so that the cadence could not be high. Moreover, this instrument only lasted for less than two years during solar minimum, making it not that useful for CME studies.

The Coronal Multichannel Polarimeter (CoMP) (Tomczyk *et al.*, 2008) is also such an instrument. It uses a narrow-band tunable filter to take high-cadence observations of the polarization state at a few spectral locations across the profiles of three infrared lines (Fe XIII 1074.7 nm & 1079.8 nm, He I 1083.0 nm). Images taken by CoMP have a field of view (FOV) of 1.05-1.40 solar radii, a spatial resolution of 4.46″/pixel, and a typical cadence of 30 s. The instrument was initially deployed at the Sacramento Peak Observatory of the National Solar Observatory in 2004. Several successful observations of coronal Alfvén waves (Tomczyk *et al.*, 2007; Tomczyk and McIntosh, 2009) and coronal cavities (Schmit *et al.*, 2009; Dove *et al.*, 2011) have been performed since then. The instrument was recently moved to MLSO and started to do almost daily routine observations since October 2010.

Since CoMP can provide simultaneous measurements of the coronal line intensity, Doppler shift, line width, linear/circular polarization, and coronal density, it actually opens a completely new window for observations of the solar corona and CMEs. Here we report the first results of CoMP observations of CMEs. These observations might bring new insights into the initiation process of CMEs.

2. Data reduction and correction

Here we mainly use the three-point (sampled at three spectral locations 1074. 50 nm, 1074. 62 nm, 1074. 74 nm) data of the Fe XIII 1074.7 nm line taken after December 2011. In these observations, sequences of the polarization (Stokes I, Q and U only) images were obtained at each of these three spectral locations at a cadence of approximately 30 s. In this paper we mainly focus on the intensity (Stokes-I) data.

Although there are measurements at only three spectral locations, the intensity profile is in principle the same as the spectral line profile obtained by spectrographs. Thus, we can simply apply a least-squares single Gaussian fit to each intensity profile and obtain the line center intensity, central wavelength, and line width (Tomczyk *et al.*, 2007; Tomczyk and McIntosh, 2009). However, it takes too much time to apply the Gaussian fit to all intensity profiles in the full FOV for hundreds of frames. Fortunately, we found that a simple analytical solution can be derived from the three-point measurement. It is far more efficient to derive the line parameters by using the analytical solution.

If I_1, I_2, and I_3 are the measured intensities at known wavelengths (spectral locations) λ_1, λ_2, and λ_3, we have the following set of three equations:

$$I_1 = ie^{\frac{-(\lambda_1-\lambda_0)^2}{w^2}}, \tag{1}$$

$$I_2 = ie^{\frac{-(\lambda_2-\lambda_0)^2}{w^2}}, \tag{2}$$

$$I_3 = ie^{\frac{-(\lambda_3-\lambda_0)^2}{w^2}}, \tag{3}$$

It is clear that there are only three unknowns: the line center intensity i, center wavelength (λ_0), and exponential line width (w). So we should be able to directly derive these three unknowns from the three equations. If we take the natural log of the ratios I_3/I_2 and I_1/I_2 and denote them as a and b, we have:

$$a = ln(\tfrac{I_3}{I_2}) = \tfrac{-(\lambda_3-\lambda_0)^2}{w^2} + \tfrac{(\lambda_2-\lambda_0)^2}{w^2}, \tag{4}$$

$$b = ln(\tfrac{I_1}{I_2}) = \tfrac{-(\lambda_1-\lambda_0)^2}{w^2} + \tfrac{(\lambda_2-\lambda_0)^2}{w^2}, \tag{5}$$

If we take the sum $a + b$ and define δ as the spectral pixel size (λ_2-λ_1 or λ_3-λ_2), the line width can be derived and expressed as:

$$w = \sqrt{\tfrac{-2\delta}{a+b}}. \tag{6}$$

If λ_2 happens to be the rest wavelength, we can derive the Doppler shift by taking the difference $a - b$:

$$v = \lambda_0 - \lambda_2 = \tfrac{w^2}{4\delta}(a - b). \tag{7}$$

Finally, the line center intensity can be computed as:

$$i = I_2 e^{\frac{v^2}{w^2}}. \tag{8}$$

We show in Figure 1 three examples of observed intensity profiles and the line parameters derived by using the analytical solution. The solid line in each panel is the Gaussian function constructed by using the derived line parameters (we call it analytical Gaussian fit). Here a positive and negative values of the Doppler shift mean red shift (away from the Earth) and blue shift (towards the Earth), respectively.

Once we derive the line parameters for each intensity profile in the FOV, we can produce maps of intensity, Doppler shift, and line width. Maps generated from observations at different times can then be used to make movies of intensity, Doppler shift, and line width.

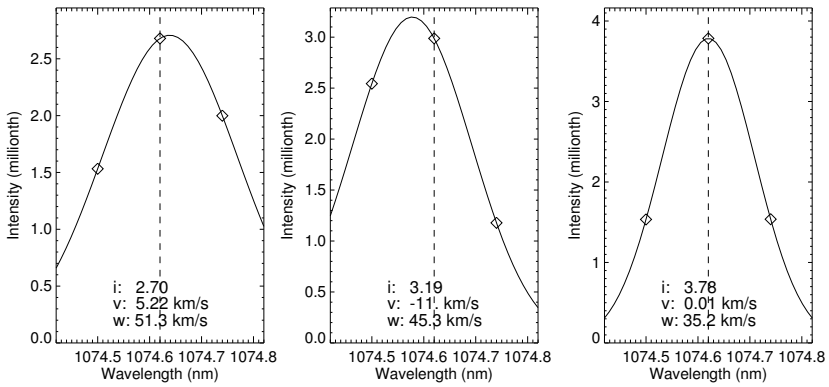

Figure 1. Three examples of observed emission line profiles (diamonds) and the analytical Gaussian fits (solid line). The dashed line indicates the rest wavelength of the line. The line center intensity (i), Doppler shift (v) and line width (w) are marked in each panel.

The Doppler shift maps usually show predominant blue shift at east limb and red shift at west limb, which suggests a east-west trend in the line of sight (LOS) Doppler shift. This trend is at least partly caused by the rotation of the solar corona. We calculate the median value of Doppler shift at each Solar-X location to produce the east-west trend (Doppler shift as a function of Solar-X). A median filter is then applied to this trend to eliminate possible abnormal values. Then we apply a fifth order polynomial fit to the filtered trend. The resulting smooth trend is then subtracted from the map of Doppler shift.

Since there is no calibration lamp or cold lines, we could not perform an absolute wavelength calibration. We simply assume that the median value of Doppler shift is zero in each image. This assumption is usually valid since non-radial flows should on average cancel out each other (e.g., Hassler *et al.*, 1999,Tian *et al.*, 2010) at limb and CoMP has such a large FOV. In addition, we are only interested in large Doppler shift perturbation which is unlikely to be affected by the accuracy of the absolute wavelength scale.

3. First results of CME observations

As we mentioned previously, CoMP provides simultaneous high-cadence (30 s) observations of coronal line intensity, Doppler shift and line width in a large FOV for the first time. Such completely new types of observations may provide new insights into the processes of CME initiation and propagation. We have checked the CoMP data archive as well as the Atmospheric Imaging Assembly (AIA, Lemen *et al.*, 2012) onboard the Solar Dynamics Observatory (SDO) and SOHO/LASCO data, and found 18 obvious CMEs observed by CoMP between December 2011 and October 2012. Table 1 lists some information (observation date, approximate time when CoMP observes the CME, associated flare class, east/west side, and other features) of these CMEs.

We found that the typical characteristics of CMEs in the CoMP data are the dramatic changes of Doppler shift and the obviously enhanced line width.

Table 1. CMEs observed by CoMP between December 2011 and October 2012. The flare class is taken from Heliophysics Event Registry (http://www.lmsal.com/isolsearch).

id	date	time	flare class	side	other features
1	2011 Dec 07	20:10	C2.7?	east	loop oscillation
2	2011 Dec 30	20:18	C4.4	west	flux rope, type-II radio burst
3	2012 Jan 14	21:12	C	west	
4	2012 Mar 15	01:33	C1.1	west	
5	2012 Mar 17	23:55	B8.1	west	large-scale disturbance
6	2012 Mar 27	21:40	no flare	west	
7	2012 Apr 11	20:40	no flare	west	Dimming in STEREO-A EUVI-195
8	2012 Apr 27	17:20	no flare	east	
9	2012 May 15	17:20	no flare	west	possible reconnection at a null
10	2012 May 26	20:38	no flare	west	partial halo, originates from back side of the Sun
11	2012 Jun 01	22:16	C3.3	west	
12	2012 Jun 08	23:24	no flare	west	
13	2012 Jul 06	23:05	X1.1	west	large-scale disturbance
14	2012 Jul 13	19:45	C1.3	west	large-scale disturbance
15	2012 Aug 07	19:02	C	east	
16	2012 Aug 24	19:30	B	east	narrow eruption
17	2012 Sept 15	22:57	C9	west	
18	2012 Sept 22	19:30	B9.3	east	

Although all CMEs do show some perturbation in the image sequences of the intensity, the perturbation is much more obvious in the image sequences of the Doppler shift and line width. This is not difficult to understand since higher-order moments are usually more sensitive to changes. The significant changes of Doppler shift are probably largely associated with the coronal response to the mass eruptions and lateral expansion of CMEs. The increased line width might be caused by the enhanced flow inhomogenuity and turbulence in various substructures of CMEs in the LOS direction.

Figure 2 shows images of the three line parameters before and during the 2011 Dec 30 CME. The CME-caused changes of all line parameters can be clearly identified through a comparison between the first and second rows. Continuous evolution of different line parameters can be seen from the online movies m2a.mov (full FOV) and m2b.mov (partial FOV). The outward propagating ejecta causes a dimming of $\sim$50% in the intensity, shifts the line center by about 20 km/s blueward, and enhances the line width by $\sim$20 km/s. The spatial pattern of the intensity change roughly coincides with those of the Doppler shift and line width enhancement.

From LASCO movies (http://lasco-www.nrl.navy.mil/daily_mpg/), we can see that this CME developed into a ring-shaped propagating feature in the FOV of LASCO-C2 & C3. Such a feature is likely to be a signature of flux rope or

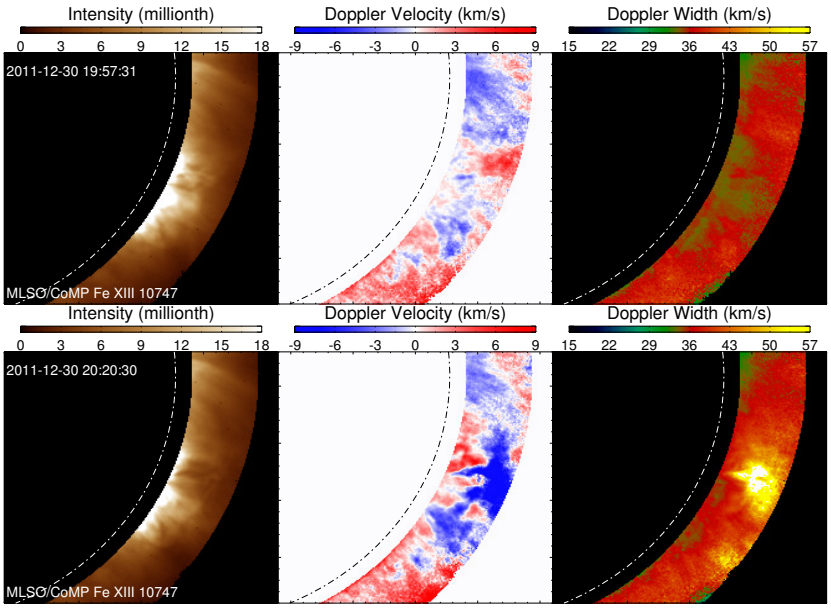

Figure 2. An eruption observed by CoMP on 2011 Dec 30. The first and second rows show images of the line center intensity, Doppler shift and line width at 19:57:31 (before eruption) and 20:20:30 UT (during eruption), respectively. The dot-dash line in each panel marks the limb of the solar disk. Two online movies (m2a.mov, m2b.mov) are associated with this figure.

magnetic cloud (e.g., DeForest, Howard, and Tappin, 2011). From Figure 2 we can see that this CME possibly erupts from an active region (AR). It is not clear whether the flux rope exists prior to eruption or forms during the eruption.

A possible flux rope is also identified from the LASCO-C2 & C3 movies on 2011 Oct 13. From AIA images, we can see that this flux rope-type CME seems to originate from a coronal cavity at the northwest limb. Such a connection favors the flux-rope interpretation of coronal cavities (Low and Hundhausen, 1995; Gibson *et al.*, 2006). Unfortunately, the CoMP data is only available prior to the CME eruption and part of the cavity is blocked by the instrument ear (Steve: please define it). We hope that future observations may catch the complete process of flux rope formation and eruption.

The intensity perturbation of the 2012 March 27 CME is very small, which might be due to the fact that the CME propagates largely off the plane of sky (POS). Despite the weak signal in the intensity, we see obvious change of the Doppler shift and line width. From Figure 3 and the online movie m3.mov we can clearly see the significant perturbation of Doppler shift and line width as the CME propagates into the FOV of CoMP.

The 2011 Dec 7 eruption only revealed very weak perturbation in the daily LASCO-C2 & C3 movies. However, as we can see from Figure 4 & Figure 5, this eruption was clearly recorded by both CoMP & SDO/AIA. The dominant ions in the 304Å, 171Åand 193Å passbands are He II, Fe IX, and Fe XII, respectively (O'Dwyer *et al.*, 2010). The AIA data seems to suggest that this is a failed or at least partial eruption, which might explain the fact that the event is hardly

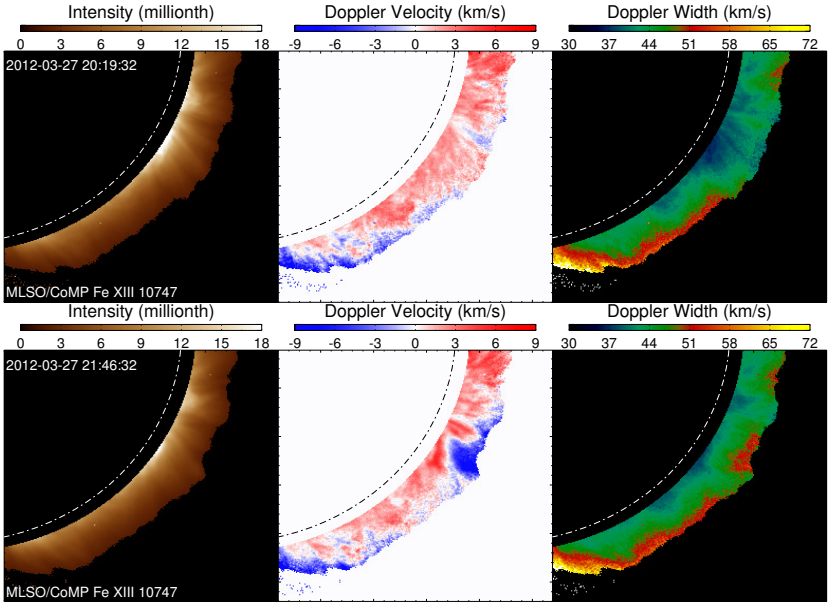

Figure 3. An eruption observed by CoMP on 2012 March 27. The first and second rows show images of the line center intensity, Doppler shift and line width at 20:19:32 (before eruption) and 21:46:32 UT (during eruption), respectively. The dot-dash line in each panel marks the limb of the solar disk. An online movies (m3.mov) is associated with this figure.

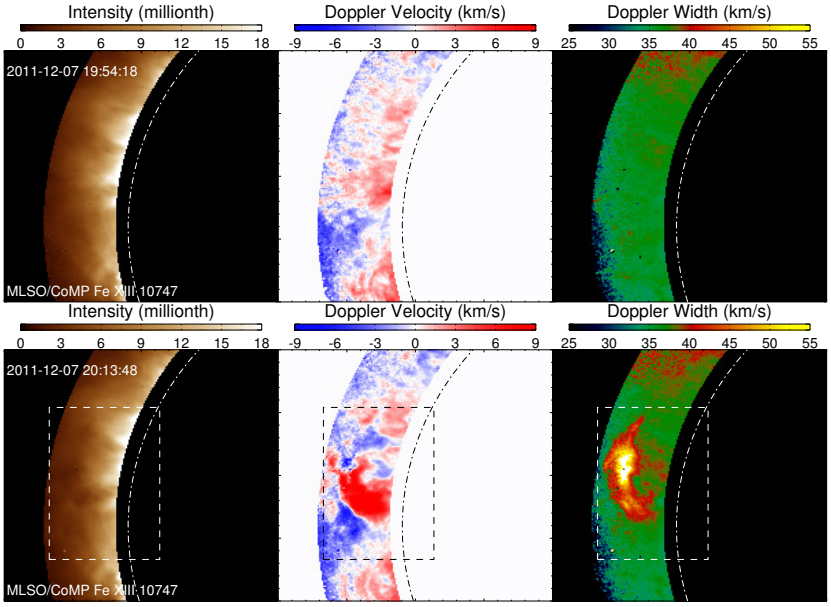

Figure 4. An eruption observed by CoMP on 2011 Dec 7. The first and second rows show images of the line center intensity, Doppler shift and line width at 19:54:18 and 20:13:48 UT, respectively. The dot-dash line in each panel marks the limb of the solar disk. The rectangular region indicates the field of view shown in Figure 5. An online movies (m4.mov) is associated with this figure.

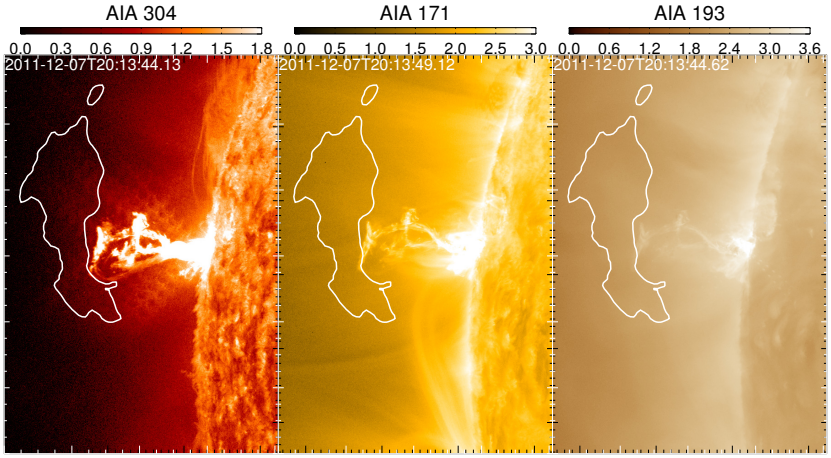

Figure 5. AIA observations of the 2011 Dec 7 event. Images of the AIA 304Å, 171Å and 193 Å passbands around 20:13:48 are presented from left to right. The contours mark locations where the line width of Fe XIII 1074.7 nm is larger than 42 km/s.

identified from the LASCO data. The eruption appears as a dark propagating feature in the CoMP intensity data, as can be seen from Figure 4 and the online movie m4.mov. The eruption also shifts the line center by about 20 km/s redward and enhances the line width by more than ∼20 km/s. The dark feature roughly coincides with the enhanced line width and largely perturbed Doppler shift.

In Figure 5 we present the high-resolution AIA images at three passbands. These images were taken around 20:13:48 UT, the time when the images in the lower panel of Figure 5 were taken. The most enhanced line width (larger than 42 km/s) region, which is also approximately the region where the most significant perturbation of the line center intensity and Doppler shift occurs, is outlines by the white contours in each panel. It seems that this region is right ahead of the ejecta. A comparison between Figure 4 and Figure 5 suggests that the ejecta itself is also associated with large changes of Doppler shift and enhancement of the line width. But these changes are clearly not as prominent as those ahead of the ejecta. The large perturbation ahead of the ejecta is likely largely caused by the blastic disturbance of the plasma and magnetic environment around the leading edge of the fast ejection.

Interestingly, we do not see any dark propagating feature ahead of this ejecta in the AIA movies (not shown here). It is known that all of these three passbands of AIA have significant contribution from emission of cooler materials, whereas the CoMP emission is almost purely from the hot Fe XIII ion. But it is still not clear how the perturbation ahead of the ejecta causes a reduction in the intensity of Fe XIII 1074.7 nm but no discernible change in the AIA images.

Another interesting aspect of the 2011 Dec 7 eruption is the transverse oscillation of a loop system excited by the ejecta. The loop oscillation is best seen in the AIA 171Å movie (not shown here). The oscillating loop is clearly present in Figure 5 and is about 432 Mm in length. The oscillation has a period of

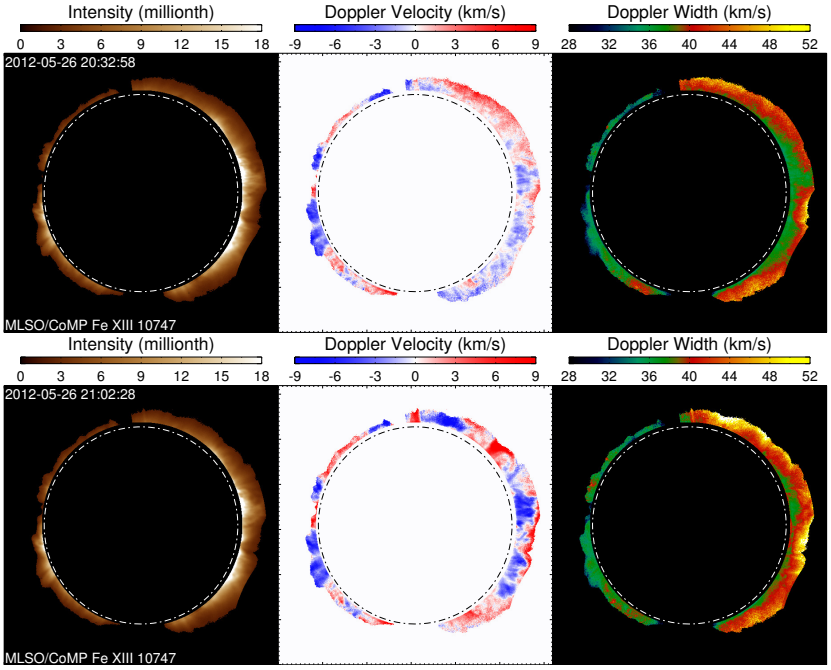

Figure 6. A partial halo-CME observed by CoMP on 2012 May 26. The first and second rows show images of the line center intensity, Doppler shift and line width at 20:32:58 and 21:02:28 UT, respectively. The dot-dash line in each panel marks the limb of the solar disk. An online movies (m6.mov) is associated with this figure.

about 15 minutes and lasts for 4 cycles before damping out. The kink speed (twice the loop length divided by the period) at the apex of this oscillating loop can thus be calculated as 960 km/s. According to Edwin and Roberts, 1983, the Alfvén speed inside the oscillating loop can be constraint to the range of $960/\sqrt{2}$ km/s-960 km/s. The two Fe XIII lines used by CoMP (1074.7 nm & 1079.8 nm) can in principle be used to diagnose the coronal electron density. Combining information of the Alfvén speed and electron density, we can directly calculate the coronal magnetic field strength. Unfortunately, this oscillating loop is barely resolved by CoMP. In addition, the density diagnostics of CoMP is still not finalized. We are planning to do joint observations of HINODE/EIS (Culhane *et al.*, 2007) and CoMP, trying to use the density diagnostics of EIS to calibrate that of CoMP.

Figure 6 shows snapshots of CoMP observations of a partial halo-CME. A complete halo is seen at the viewpoint of STEREO-A. This eruption seems to originate from the backside of the Sun and propagates away from the Sun. The quickly-developed large-scale disturbance can be clearly identified from movies of the Doppler shift and line width (mainly at the west limb). Figure 6 clearly shows that the perturbation in the intensity data is not as significant as in the Doppler shift and line width, probably because of the strong foreground and background coronal emission. The quickly-developed perturbation might be associated with the propagation of "EUV waves". Chen, Ding, and Chen, 2010

suggests that spectroscopic observations may be used to identify the nature of "EUV waves", namely fast waves (e.g., Patsourakos and Vourlidas, 2009) or non-wave phenomenon such as successive stretching of magnetic field lines (e.g., Chen *et al.*, 2002). Thus, combing numerical simulations and the spectroscopic-like large-FOV CoMP observations might reveal more insights into the process of "EUV waves".

CoMP observations of the 2012 May 26 CME suggest the importance of monitoring space weather at ground. The 2012 May 26 CME first appears as a partial halo in the FOV of LASCO-C2 at 20:57, which is about 20 minutes later than the time (20:38 UT) when CoMP observes the larger-scale perturbation in the coronal line width and Doppler shift. So it is already clear that CoMP observations can be very important for the prediction of Earth-directed halo CMEs. In this sense, observations of halo-CMEs by ground-based instruments like CoMP provide a cheap and low-risk means of space weather monitoring.

4. Summary and future perspective

CoMP provides high-cadence large-FOV spectroscopic-like observations of CMEs for the first time. We have presented first results of CME observations by CoMP in this paper. Our results show that the primary characteristics of CMEs are the dramatic change of the Doppler shift and obviously enhanced line width. The information provided by these CoMP observations may be important for our better understanding of various CME processes such as the formation of flux ropes and propagation of "EUV waves". Ground based CoMP observations have also provided a cheap and low-risk means of space weather monitoring. So far we have identified 18 obvious CMEs in the CoMP data. With the increase of the solar activity, we expect to observe more CMEs in the future.

CoMP observations of CMEs are not restricted to the images of line center intensity, Doppler shift and line width. In fact CoMP measures the complete polarization state of three emission lines. The linear (Stokes-Q & U) and circular (Stokes-V) polarization data are not used in our analysis because we do not find significant change of the linear polarization signal during CME eruptions and the circular polarization signal is too weak under current observing programs. We plan to adjust the observing programs and perform detailed analysis of the linear and circular polarization data in the near future.

As we mentioned above, the density diagnostics using the two Fe XIII lines is underway. Once this is finalized, we should be able to study density changes during CMEs, which could be used to estimate the CME mass (Harrison *et al.*, 2003,Jin *et al.*, 2009,Tian *et al.*, 2012). In addition, combining the density diagnostics and the Alfvén wave (Doppler shift oscillation) analysis (Tomczyk *et al.*, 2007; Tomczyk and McIntosh, 2009; McIntosh, de Pontieu, and Tomczyk, 2008), we can produce maps of the electron density, Alfvén speed and magnetic field strength before and after CMEs. Such information can be used to constrain background coronal parameters prescribed in models of CMEs.

CoMP is just a prototype of the Large-aperture Coronagraph component of the proposed COronal Solar Magnetism Observatory (COSMO). With a FOV

of 1.05-2.0 solar radii, COSMO can greatly expand the ability of CME observations by CoMP. In addition, the Chromosphere and Prominence Magnetometer (ChroMag) component of COSMO can monitor solar activities on the disk. Thus, a combination of both components is likely to monitor the complete process of (halo) CME initiation and early-phase propagation.

Acknowledgements SDO is the first mission of NASAs Living With a Star (LWS) Program. H. Tian's work at CfA is supported by NASA grant. Part of this work is done at NCAR, where H. Tian is supported by the ASP Postdoctoral Fellowship Program. The National Center for Atmospheric Research is sponsored by the National Science Foundation.

References

Brueckner, G.E., Howard, R.A., Koomen, M.J., Korendyke, C.M., Michels, D.J., Moses, J.D., Socker, D.G., Dere, K.P., Lamy, P.L., Llebaria, A., Bout, M.V., Schwenn, R., Simnett, G.M., Bedford, D.K., Eyles, C.J.: 1995, The Large Angle Spectroscopic Coronagraph (LASCO). *Solar Phys.* **162**, 357 – 402. doi:10.1007/BF00733434.

Chen, F., Ding, M.D., Chen, P.F.: 2010, Spectroscopic Analysis of an EIT Wave/dimming Observed by Hinode/EIS. *Astrophys. J.* **720**, 1254 – 1261. doi:10.1088/0004-637X/720/2/1254.

Chen, P.F., Wu, S.T., Shibata, K., Fang, C.: 2002, Evidence of EIT and Moreton Waves in Numerical Simulations. *Astrophys. J. Lett.* **572**, L99 – L102. doi:10.1086/341486.

Culhane, J.L., Harra, L.K., James, A.M., Al-Janabi, K., Bradley, L.J., Chaudry, R.A., Rees, K., Tandy, J.A., Thomas, P., Whillock, M.C.R., Winter, B., Doschek, G.A., Korendyke, C.M., Brown, C.M., Myers, S., Mariska, J., Seely, J., Lang, J., Kent, B.J., Shaughnessy, B.M., Young, P.R., Simnett, G.M., Castelli, C.M., Mahmoud, S., Mapson-Menard, H., Probyn, B.J., Thomas, R.J., Davila, J., Dere, K., Windt, D., Shea, J., Hagood, R., Moye, R., Hara, H., Watanabe, T., Matsuzaki, K., Kosugi, T., Hansteen, V., Wikstol, Ø.: 2007, The EUV Imaging Spectrometer for Hinode. *Solar Phys.* **243**, 19 – 61. doi:10.1007/s01007-007-0293-1.

DeForest, C.E., Howard, T.A., Tappin, S.J.: 2011, Observations of Detailed Structure in the Solar Wind at 1 AU with STEREO/HI-2. *Astrophys. J.* **738**, 103. doi:10.1088/0004-637X/738/1/103.

Dove, J.B., Gibson, S.E., Rachmeler, L.A., Tomczyk, S., Judge, P.: 2011, A Ring of Polarized Light: Evidence for Twisted Coronal Magnetism in Cavities. *Astrophys. J. Lett.* **731**, L1. doi:10.1088/2041-8205/731/1/L1.

Edwin, P.M., Roberts, B.: 1983, Wave propagation in a magnetic cylinder. *Solar Phys.* **88**, 179 – 191. doi:10.1007/BF00196186.

Gibson, S.E., Foster, D., Burkepile, J., de Toma, G., Stanger, A.: 2006, The Calm before the Storm: The Link between Quiescent Cavities and Coronal Mass Ejections. *Astrophys. J.* **641**, 590 – 605. doi:10.1086/500446.

Gosling, J.T., McComas, D.J., Phillips, J.L., Bame, S.J.: 1991, Geomagnetic activity associated with earth passage of interplanetary shock disturbances and coronal mass ejections. *J. Geophys. Res.* **96**, 7831 – 7839. doi:10.1029/91JA00316.

Harrison, R.A., Bryans, P., Simnett, G.M., Lyons, M.: 2003, Coronal dimming and the coronal mass ejection onset. *Astron. Astrophys.* **400**, 1071 – 1083. doi:10.1051/0004-6361:20030088.

Hassler, D.M., Dammasch, I.E., Lemaire, P., Brekke, P., Curdt, W., Mason, H.E., Vial, J.-C., Wilhelm, K.: 1999, Solar Wind Outflow and the Chromospheric Magnetic Network. *Science* **283**, 810. doi:10.1126/science.283.5403.810.

Jin, M., Ding, M.D., Chen, P.F., Fang, C., Imada, S.: 2009, Coronal Mass Ejection Induced Outflows Observed with Hinode/EIS. *Astrophys. J.* **702**, 27 – 38. doi:10.1088/0004-637X/702/1/27.

Lemen, J.R., Title, A.M., Akin, D.J., Boerner, P.F., Chou, C., Drake, J.F., Duncan, D.W., Edwards, C.G., Friedlaender, F.M., Heyman, G.F., Hurlburt, N.E., Katz, N.L., Kushner, G.D., Levay, M., Lindgren, R.W., Mathur, D.P., McFeaters, E.L., Mitchell, S., Rehse,

R.A., Schrijver, C.J., Springer, L.A., Stern, R.A., Tarbell, T.D., Wuelser, J.-P., Wolfson, C.J., Yanari, C., Bookbinder, J.A., Cheimets, P.N., Caldwell, D., Deluca, E.E., Gates, R., Golub, L., Park, S., Podgorski, W.A., Bush, R.I., Scherrer, P.H., Gummin, M.A., Smith, P., Auker, G., Jerram, P., Pool, P., Soufli, R., Windt, D.L., Beardsley, S., Clapp, M., Lang, J., Waltham, N.: 2012, The Atmospheric Imaging Assembly (AIA) on the Solar Dynamics Observatory (SDO). *Solar Phys.* **275**, 17 – 40. doi:10.1007/s11207-011-9776-8.

Low, B.C., Hundhausen, J.R.: 1995, Magnetostatic structures of the solar corona. 2: The magnetic topology of quiescent prominences. *Astrophys. J.* **443**, 818 – 836. doi:10.1086/175572.

McIntosh, S.W., de Pontieu, B., Leamon, R.J.: 2010, The Impact of New EUV Diagnostics on CME-Related Kinematics. *Solar Phys.* **265**, 5 – 17. doi:10.1007/s11207-010-9538-z.

McIntosh, S.W., de Pontieu, B., Tomczyk, S.: 2008, A Coherence-Based Approach for Tracking Waves in the Solar Corona. *Solar Phys.* **252**, 321 – 348. doi:10.1007/s11207-008-9257-x.

Mierla, M., Schwenn, R., Teriaca, L., Stenborg, G., Podlipnik, B.: 2005, Using LASCO-C1 spectroscopy for coronal diagnostics. *Advances in Space Research* **35**, 2199 – 2203. doi:10.1016/j.asr.2005.04.031.

O'Dwyer, B., Del Zanna, G., Mason, H.E., Weber, M.A., Tripathi, D.: 2010, SDO/AIA response to coronal hole, quiet Sun, active region, and flare plasma. *Astron. Astrophys.* **521**, A21. doi:10.1051/0004-6361/201014872.

Patsourakos, S., Vourlidas, A.: 2009, "Extreme Ultraviolet Waves" are Waves: First Quadrature Observations of an Extreme Ultraviolet Wave from STEREO. *Astrophys. J. Lett.* **700**, L182 – L186. doi:10.1088/0004-637X/700/2/L182.

Schmit, D.J., Gibson, S.E., Tomczyk, S., Reeves, K.K., Sterling, A.C., Brooks, D.H., Williams, D.R., Tripathi, D.: 2009, Large-Scale Flows in Prominence Cavities. *Astrophys. J. Lett.* **700**, L96 – L98. doi:10.1088/0004-637X/700/2/L96.

Tian, H., Tu, C., Marsch, E., He, J., Kamio, S.: 2010, The Nascent Fast Solar Wind Observed by the EUV Imaging Spectrometer on Board Hinode. *Astrophys. J. Lett.* **709**, L88 – L93. doi:10.1088/2041-8205/709/1/L88.

Tian, H., McIntosh, S.W., Xia, L., He, J., Wang, X.: 2012, What can We Learn about Solar Coronal Mass Ejections, Coronal Dimmings, and Extreme-ultraviolet Jets through Spectroscopic Observations? *Astrophys. J.* **748**, 106. doi:10.1088/0004-637X/748/2/106.

Tomczyk, S., McIntosh, S.W.: 2009, Time-Distance Seismology of the Solar Corona with CoMP. *Astrophys. J.* **697**, 1384 – 1391. doi:10.1088/0004-637X/697/2/1384.

Tomczyk, S., McIntosh, S.W., Keil, S.L., Judge, P.G., Schad, T., Seeley, D.H., Edmondson, J.: 2007, Alfvén Waves in the Solar Corona. *Science* **317**, – . doi:10.1126/science.1143304.

Tomczyk, S., Card, G.L., Darnell, T., Elmore, D.F., Lull, R., Nelson, P.G., Streander, K.V., Burkepile, J., Casini, R., Judge, P.G.: 2008, An Instrument to Measure Coronal Emission Line Polarization. *Solar Phys.* **247**, 411 – 428. doi:10.1007/s11207-007-9103-6.

Wang, Y.M., Ye, P.Z., Wang, S., Zhou, G.P., Wang, J.X.: 2002, A statistical study on the geoeffectiveness of Earth-directed coronal mass ejections from March 1997 to December 2000. *Journal of Geophysical Research (Space Physics)* **107**, 1340. doi:10.1029/2002JA009244.

Zhang, J., Richardson, I.G., Webb, D.F., Gopalswamy, N., Huttunen, E., Kasper, J.C., Nitta, N.V., Poomvises, W., Thompson, B.J., Wu, C.-C., Yashiro, S., Zhukov, A.N.: 2007, Solar and interplanetary sources of major geomagnetic storms (Dst=-100 nT) during 1996-2005. *Journal of Geophysical Research (Space Physics)* **112**(11), 10102. doi:10.1029/2007JA012321.